I. J. Trans. Phenomena, 3(4):437–448

1028-6578/01 $12.00 + .00

Numerical Simulation of Jet Impingement/Channel Flow Cooling of an Array of Heated Strips by a Fluorinert Liquid

MASUD BEHNIA[a], JAN PRALITS[b], and WATARU NAKAYAMA[c,*]

[a]*School of Mechanical and Manufacturing Engineering, The University of New South Wales Sydney, Australia;* [b]*Department of Mechanics, The Royal Institute of Technology, Stockholm, Sweden;* [c]*ThermTech International, Kanagawa, Japan*

(Received 26 February 2001; In final form 17 June 2001)

Numerical simulations have been performed to investigate the heat transfer characteristics of microelectronic chips submerged in a fluorinert liquid (FX3250), and the results are compared with the experimental data. The chip array is simulated by five 4 mm × 35 mm heater strips, with the middle strip facing a 1 mm-wide slot nozzle and the remaining strips being placed symmetrically with respect to the nozzle. Turbulence and near-wall flow behaviour are modelled using various turbulence models. The average heat transfer coefficient is calculated for each strip and is correlated with the strip width-based Reynolds number, which was varied between 6000 and 90,000. It has been found that the RNG k-ε turbulence model in conjunction with a two-layer near-wall treatment gives the best agreement with the experimental data for the middle strip. However, for the other strips, it was found that all the turbulence models do not properly capture the trend of the experimental data. This paper highlights the capability and limitations of a CFD code in simulating heat transfer in constrained space of electronic equipment.

Keywords: Computational fluid dynamics; Jet impingement cooling; Dielectric liquid cooling; Heated strips; Turbulent forced convection

INTRODUCTION

From portable computers to massively parallel processors, squeezing microelectronic chips and other components into constrained space has become the norm of today's packaging design. For higher classes of computers such as server computers and supercomputers, further compact packaging is made possible only when we resort to liquid cooling (Nakayama, 1997). This method of cooling has been a major subject for thermal management research for many years, but there have been only a few

*Address correspondence to: Dr. Wataru Nakayama, ThermTech International, 920-7 Higashi Kosio, Oh-Iso Machi, Kanagawa 255-0004, Japan, E-mail: WatNAKAYAMA@aol.com

instances of commercial applications. Previous studies on liquid cooling, the list of which is too exhaustive to be listed here, mainly focused on heat transfer on the chip assuming little spatial constraint around the chip. Without spatial constraint, there is a certain range of options in choosing a cooling method. For example, a low thermal resistance normally accorded to liquid cooling can also be realized by a high-speed air flow coupled with a large heat sink (Nakayama, 1997). In such cases, air-cooling is often favoured over liquid cooling as testified by recent designs of server computers. So, competitiveness of liquid cooling vis-a-viz air cooling depends much on circumstantial imperatives rather than the heat transfer coefficient on the chip's surface. Unpopularity of liquid cooling in commercial equipment is a manifestation of the fact that the circumstance for liquid cooling has not matured enough until now.

Now expecting emerging needs for liquid cooling some studies have been conducted assuming spatial constraints; Schafer *et al.* (1991), Willingham and Mudawar (1992), Mudawar and Wadsworth (1991). In these studies, a single row of simulated chips was placed in a narrow channel (Schafer *et al.*, 1991; Willingham and Mudawar, 1992), or the chips are cooled by individual impinging jets (Mudawar and Wadsworth, 1991). Individual chip-wise or row-wise cooling makes the thermal field around the chips relatively simple, however, at the expense of the system cost. The hardware becomes more elaborate as the coolant route comes to have a greater number of branches in individual cooling. Having abreast this issue, Nakayama *et al.* (1996) studied the case of collective cooling for a chip array. Figure 1 shows a system envisioned in their study. Chips are spread on a card, and the card is encased in a thin channel that has a slot nozzle in the middle of the wall. The coolant is introduced through the nozzles, impinges on the chips in the middle row, and flows in the channels to the exits. The nozzle extends over the whole width (normal to the paper) of the card, so the chips are cooled collectively. The next section describes the experimental apparatus in some detail.

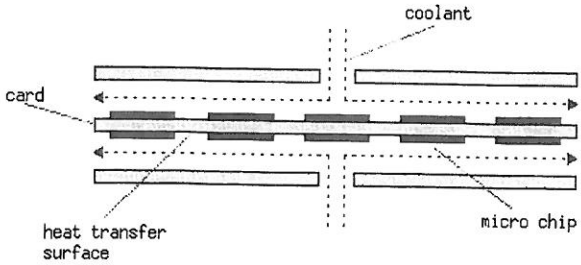

FIGURE 1 A typical card system modeled by Nakayama *et al.* (1996).

Collective chip cooling in constrained space, however, poses a challenge. Since the experiment is in general costly and time-consuming, we need to run computational fluid dynamics (CFD) simulations to understand the effects of various parameters involved in design. The challenge is in the complexity of coolant flow that arises due to involvement of disparate length scales in the coolant channel. For example, the channel of our interest has a high aspect ratio, thin in the direction normal to the chip array but wide in a plane parallel to the chip array. Besides, the coolant inlet is provided in a constrained space, and the inlet flow is not well rectified. A flow in such a space has a three-dimensional structure (Nakayama *et al.*, 1996), and when it is in the turbulent regime, there is a considerable uncertainty in the adequacy of turbulence models incorporated in the CFD code.

So, when we use the CFD code in simulations, we must be aware of its capability as well as limitations. Since, in our view, the turbulence modelling has not yet been advanced to a satisfactory level, we must accept a certain level of tolerance in engineering computations. In this paper the results of CFD simulations are compared with the experimental data, not for benchmarking of conventional sense but to find a capability of a commercial CFD code in simulating coolant flows and heat transfer in a constrained space.

A SIMULATED CHIP ARRAY COOLED BY JET/CHANNEL FLOW

Nakayama *et al.* (1996) performed impingement jet/channel flow experiments for single phase and boiling

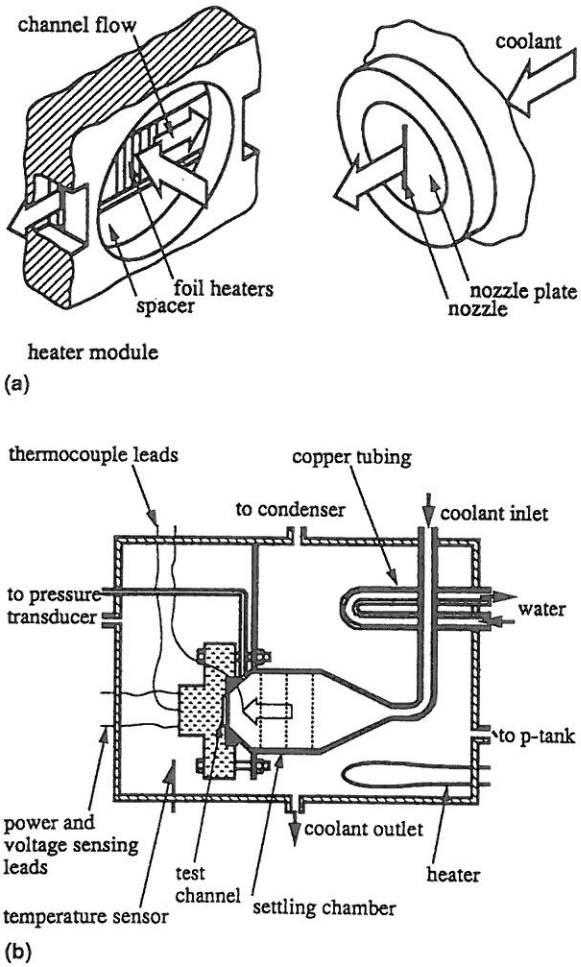

FIGURE 2 Test piece and experimental apparatus of Nakayama *et al.* (1996), a) coolant flow paths, b) assembly in the main tank.

conditions using a dielectric coolant FX3250. The experiments were motivated by the prospect of incorporating the results into emerging cooling system morphology. In such systems it is required to make the coolant flow paths compatible with the space constraints of the electrical equipment. To increase the heat transfer coefficient and minimise the temperature rise of the coolant, short flow paths are used (Figure 1). Figure 2 shows a sketch of the apparatus. A column of chips was simulated by a constantan foil strip, 35 mm long, 4 mm wide and 10 μm thick. Five such strips were mounted on a 35 mm × 100 mm bakelite plate with a 1 mm spacing between the strips. Sectional views of the assembly are shown in Figure 2(a). Opposite the bakelite plate is a circular 2 mm thick nozzle plate in which a 35 mm × 1 mm slot is machined. The channel spacing is set by a 2 mm spacer between the bakelite plates. The nozzle inlet velocity, V_j, was varied from 0.7 to 5.3 m/s and the nozzle inlet temperature, T_j, was held at 36, 46 or 54°C, i.e. 20, 10 and 2°C of subcooling (FX3250 boils at 56°C at atmospheric pressure). As shown in Figure 3 the centre of the strips were positioned at $x/B = 0, 5, 10$ from the symmetry line in each direction. The data obtained from the experiments performed by Nakayama *et al.* (1996) is essentially the relationship between the heat flux and the difference between the average temperature on the strip and the jet inlet temperature. The data was reduced to determine the mean Nusselt number based on the strip width, L:

$$\overline{\mathrm{Nu}}_L = \frac{\bar{h}L}{\lambda} \tag{1}$$

where λ is the thermal conductivity of the fluid and $\bar{h}$ is the mean heat transfer coefficient for one strip. The non-dimensional group $\overline{\mathrm{Nu}}_L/\mathrm{Pr}^{0.4}$ can then be derived as a function of the strip width-based Reynolds number, Re_L:

$$\frac{\overline{\mathrm{Nu}}_L}{\mathrm{Pr}^{0.4}} = A\mathrm{Re}_L^P \tag{2}$$

where Pr is the fluid Prandtl number and A and P are constants. No significant dependence of the data on the inlet temperature, T_j, was found. P from Eq. 2 was 0.5 under the impingement jet showing a typical laminar boundary layer type behaviour. Downstream, P was large enough to suggest a turbulent channel flow type behaviour. At low Re_L the data from strip number two is close to those of the downstream strips and at high Re_L it is close to the centre strip.

THE GEOMETRY AND CFD MODELLING

Referring to the apparatus described above, the computational domains were defined. In most runs,

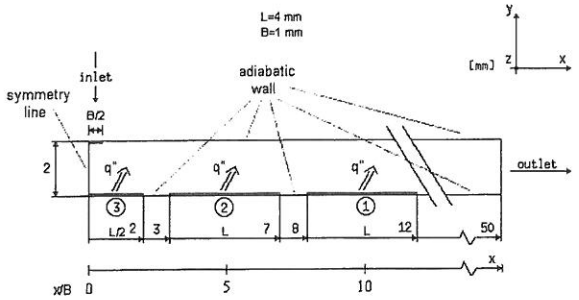

FIGURE 3 The model: B = inlet width, L = strip width, circled numbers are the strips.

the two-dimensionality of the flow is assumed. The 2D computational domain is set as 50 mm long and 2 mm thick and is shown in Figure 3. The symmetry condition is used, which allows more grid points in areas where accurate spatial resolution of the computational domain is important, i.e. where gradients are large. The circled numbers in Figure 3 denote the three heated strips. Strips number 1 and 2 are 4 mm long. Strip number 3 and the inlet slot is half its length due to symmetry. The flow in this high aspect ratio channel has some important features. The impingement zone opposite the flow inlet has suppressed turbulence at the stagnation point. The flow is wall dominated and is characterised by $y^+ < 100$ for $\mathrm{Re}_L \approx 6000$ and $y^+ < 200$ for $\mathrm{Re}_L \approx 60,000$ in most of the flow domain. The y^+ here is defined as:

$$y^+ = \frac{y}{\nu}\sqrt{\frac{\tau_w}{\rho}} \tag{3}$$

where y is the distance to the closest wall, ν is the dynamic viscosity of the fluid, ρ is the density of the fluid and τ_w is the shear stress at the wall. The near wall treatment becomes extremely important as virtually all of the flow is within the viscous boundary layer. The flow at the heater strips is developing, which means that the flow field also varies in the direction of the flow.

The numerical simulations were performed using the Fluent CFD code. It uses a control volume based technique for a structured grid to solve the conservation equations for mass, momentum and energy. Fluent solves the energy equation in the form of a transport equation for the static enthalpy. The pressure and velocity fields are coupled using the SIMPLEC algorithm.

The turbulence can be simulated using k-ε type models or the Reynolds Stress Model (RSM). In fluent, in addition to the RSM there are two k-ε type models, i.e. the standard one and the RNG. The RNG model is more responsive to the effects of rapid strain and streamline curvature than the standard k-ε model. All three models were tested and the results are compared.

The near wall behaviour can be captured by using either wall functions or a two-layer model. Wall functions have the advantage of allowing a coarser mesh near the wall and generally for such computations the first grid point is placed at $y^+ \geq 25$. For this case, the near wall behaviour is captured by the wall function. In the two-layer model the near wall treatment is approached by subdividing the domain into a viscosity-affected region and a fully turbulent region. The separation between the two regions is based on a turbulent Reynolds number,

$$\mathrm{Re}_y \equiv \frac{y\rho\sqrt{k_e}}{\mu} \tag{4}$$

where y is the normal distance from the closest wall to the cell centres, k_e is the turbulence kinetic energy and μ is the dynamic viscosity. In the turbulent part of the boundary layer ($\mathrm{Re}_y > 200$), the k-ε type model is invoked. In the viscosity affected near-wall region ($\mathrm{Re}_y < 200$), a one-equation model is employed. In this approach, the grid spacing is more restrictive than the wall function case and the first grid point needs to be placed at $y^+ \sim 1$. Generally, more than 10 cells need to be located within the viscosity affected near wall region. In the computations, it is essential that the turbulent Reynolds number, Re_y, and the y^+ value in the flow domain are checked to ensure that the two layer model is properly implemented. A previous numerical study by Morris *et al.* (1996) on prediction of jet impingement heat transfer has shown that wall function underpredict the heat transfer coefficient by more than

50%. In order to improve their wall function results, they used a tedious post-processing procedure and examined several complex turbulent Prandtl number equations. In this study, for comparison purposes, we used both a wall function approach and a near-wall-zone model. In the case of wall function simulations, we placed the first mesh point at $y^+ \sim 25$ as noted previously. For the two-layer simulations the near wall mesh was made much finer in order to capture the high velocity and temperature gradients (i.e. in the area where the jet impinges and downstream on the heated strips).

BOUNDARY CONDITIONS

Due to the complexity of experiments, the conditions at the nozzle outlet such as velocity distribution and turbulent intensity were not obtained in the experiments performed by Nakayama *et al.* (1996). The flow needs a long inlet section of about 72 diameters to become fully developed (Behnia *et al.*, 1991). The settling chamber in Figure 2(b) does not allow the flow to become fully developed. Experiments performed by Wolf *et al.* (1990) show that a non-uniform velocity profile, developed in a 48.3 hydraulic diameter long rectangular pipe, increases the centreline velocity by as much as 11% relative to the average jet velocity. It is also shown that the stagnation line heat transfer for the non-uniform velocity profile is greater than that of the uniform profile. For an unconfined impinging jet geometry, Behnia *et al.* (1991) showed that a fully developed nozzle exit profile has a 15 to 30% larger heat transfer coefficient compared to velocity profiles developed within a shorter nozzle length. They also show that increasing the turbulent intensity at the nozzle exit from 1 to 6.5% enhances the heat transfer coefficient by as much as 15% at the stagnation point. In the present simulations the nozzle exit velocity profile is assumed to be uniform and the nozzle exit turbulence intensity is set at an estimated value of 10%. The jet inlet velocity was varied from 0.51 to 7.6 m/s to cover the same Re_L (6000 to 90,000) as in the experiments. Different outlet boundary conditions have been examined in experiments performed by Schafer *et al.* (1991). They show that changing the vertical position of the outlet from $x/B \approx 20$ to $x/B \approx 32$ does not change the heat transfer coefficient of the heaters placed at $x/B = 0, 5, 10$ and 15. In the simulations, both a fully developed outlet flow assumption, and a fixed static pressure assumption at the outlet, was considered. The difference in the mean heat transfer coefficient was negligible. A fixed static pressure outlet is perhaps more representative of the present geometry than a fully developed flow assumption. The foil strips were modeled with an imposed constant heat flux boundary condition. The surrounding walls such as the area between and downstream of the foil strips and the channel roof are modelled as adiabatic walls. This is due to the fact that more than 90% of the total heat generation goes to the coolant from the foil strips (Nakayama *et al.*, 1996). The coolant used in this simulation is the 3 M Performance Fluid, PF-5060, also more widely known as FX3250. Its properties are characteristic of fully fluorinated compounds. Due to the complete fluorination of these molecules, the intermolecular forces are quite low, resulting in a low heat of vaporisation. Typical properties are high density, low viscosity, low pour points and low surface tension. The liquid has a boiling point of 56°C at atmospheric pressure. Table 1 shows the properties as a function of temperature.

TABLE 1 Thermal transport properties for PF-5060

PF-5060 dielectric fluid, thermal transport properties supplied by 3 M				
T [°C]	ρ [kg/m^3]	$\nu \times 10^7$[m^2/s]	C_p [J/kgK]	λ [W/mK]
36	1646.4	3.372	1070	0.0564
46	1620.4	3.028	1086	0.0554

RESULTS AND DISCUSSION

It is known from previous works of Wolf *et al.* (1990) and Behnia *et al.* (1998) that a non-uniform velocity profile at the nozzle exit increases the heat transfer coefficient at the stagnation point. A preliminary numerical simulation was performed with the flow developing in a 2 mm long channel before entering the channel inlet. The channel length is the thickness of the inlet slot. The results showed a slight increase in the heat transfer coefficient. It is also possible to extend the computational domain into the settling chamber. However, in addition to more costly computations this requires the experimental data in this region which is not available. Morris and Garimella (1998), in their computations have included the inlet plenum and have shown that depending on the thickness of the nozzle plate there can be a vena contracta which affects the velocity profile and hence the heat transfer rate. Nevertheless, the nozzle exit velocity profile was set as uniform, which will probably underestimate the heat transfer coefficient at the stagnation point. The turbulence intensity was kept constant at an estimated value of 10% at the nozzle exit. The experimental results suggest little difference for the heat transfer coefficient when the inlet temperature was changed from 36 to 46°C. The inlet temperature of the simulation was therefore set at 36°C as there is little variation of properties with temperature. A grid dependency check was performed to ensure that the results did not vary when the mesh was refined. The initial mesh was 355 × 35 cells and the mesh was doubled in each direction until the maximum heat transfer coefficient varied by only about two percent. The finest mesh used was 1419 × 65 cells. The features of the experiments and the numerical simulations have been compared in Table 2. The Nusselt number correlation (Eq. 2) was obtained and compared with the experimental data of Nakayama *et al.* (1996) and Schafer *et al.* (1991). The comparison can be seen in Figures 4, 5 and 6 which show the heat transfer coefficient for strip number 3, 2 and 1 respectively. For comparison, results of the simulations using different turbulence models are plotted.

There is a difference in separation distance (H/B) between the experimental data sets in Table 2. Nevertheless, Schafer *et al.* (1991) show that the effect of the separation distance H/B on results for strips at $x/B = 1, 2$ and 3 is small. The numerical correlations in Figures 4, 5 and 6 which are in the

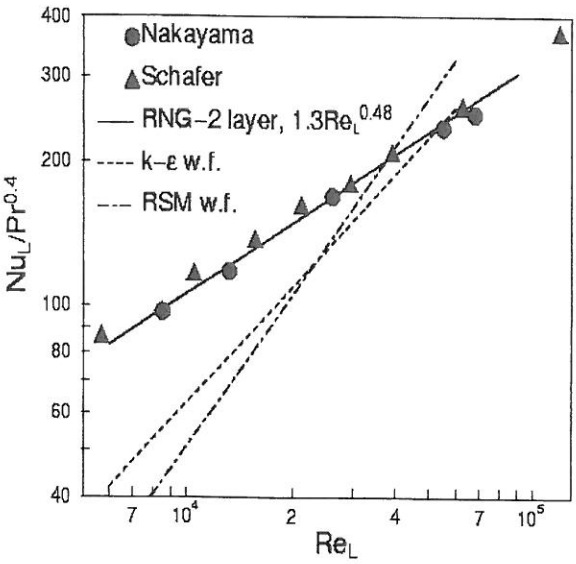

FIGURE 4 Comparison of the average heat transfer coefficient for strip No. 3, $x/B = 0$.

TABLE 2 Features of the experiments and the numerical simulation. Data: 1 Nakayama et al. (1996); 2 Schafer et al. (1991); 3 Present simulations

Data	T_j [K]	Liquid	x/B (s3,s2,s1)	H/B [-]	H [mm]	B [mm]	L [mm]	Re_L $\times 10^{-3}$[-]
1	309	FX3250	0, 5, 10	2	2	1	4	8–60
2	N/A	water	0, 5, 10	1.5	4.77	3.18	12.7	6–120
3	309	FX3250	0, 5, 10	2	2	1	4	6–90

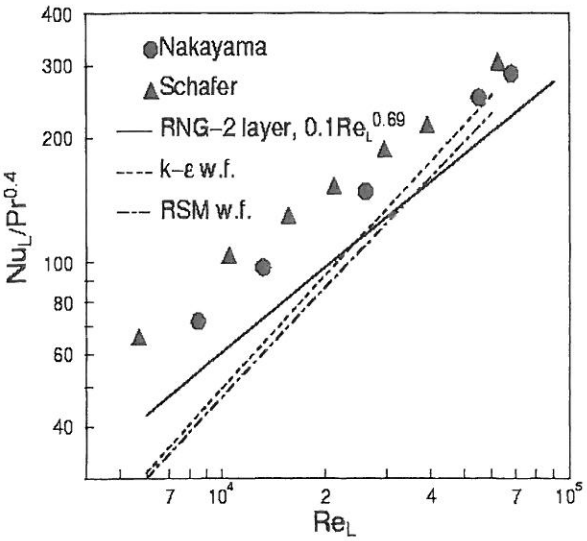

FIGURE 5 Comparison of the average heat transfer coefficient for strip No. 2, $x/B = 5$.

form of $\overline{\mathrm{Nu}_L}/\mathrm{Pr}^{0.4} = A\mathrm{Re}_L^P$ have been obtained from simulations at seven different Reynolds numbers.

The results for strip 3, $x/B = 0$, can be seen in Figure 4. It is noted that there is a very good agreement between the experimental data and the RNG k-ε two-layer simulation. The Reynolds number exponent is 0.48, which nicely matches the experimental values of 0.5 and 0.47 obtained by Nakayama *et al.* (1996) and Schafer *et al.* (1991), respectively. The exponent value of nearly 0.5 suggests a laminar type flow behaviour in this region, which was also observed in the experiments, since the strong favorable pressure gradient caused by impingement and redirection of the fluid acts to re-laminarise even a strongly turbulent flow associated with large jet velocities. The Nusselt number correlation constant A in the experiments of Nakayama *et al.* and Schafer *et al.* was 1.1 and 1.5, respectively. The difference in Nusselt number determined from experimental lines of best fit and the numerical simulation is around 4%. It is noted that, both RSM and k-ε simulations using the wall function over-predict the slope with an under-prediction of the Nusselt number at lower Reynolds numbers. A similar behaviour was also noted for the RNG k-ε simulation using the wall function. The inadequacy of wall functions in this region is not surprising as has been noted by Craft *et al.* (1993) and Morris *et al.* (1996).

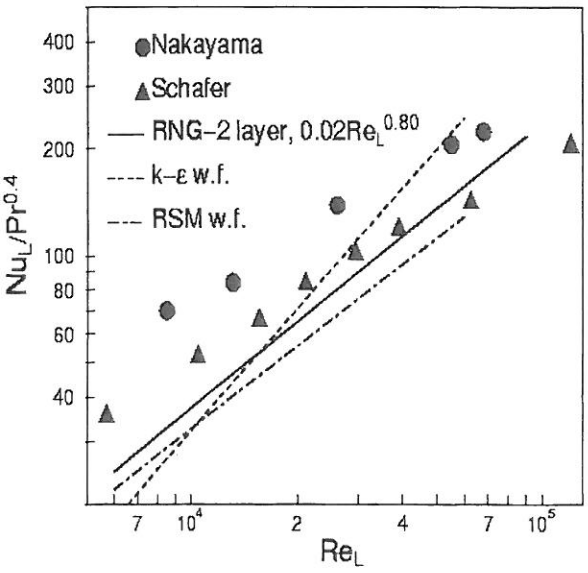

FIGURE 6 Comparison of the average heat transfer coefficient for strip No. 1, $x/B = 10$.

Figure 5 shows the results for strip 2, $x/B = 5$. The experimental Reynolds number exponents are 0.62 and 0.68 as reported by Schafer *et al.* (1991) and Nakayama *et al.* (1996), respectively. The RNG k-ε simulations yield a value of 0.69 which is in good agreement with the experiments. The value of the exponent is approaching that of a turbulent channel flow situation. This is, according to Schafer *et al.*, attributed to a recirculation zone which would enhance heat transfer by advecting warmer fluid away from the surface and increase the supply of cooler fluid on to the surface. They note that the magnitude of the heat transfer coefficient depends on where the recirculation zone is situated for each Reynolds number. Nakayama *et al.* (1996) do not state where in the flow domain the recirculation might occur and Schafer *et al.* (1991) suggest that it has its maximum at $x/B = 5$. The lower values of the non-dimensionalised Nusselt number in the RNG numerical simulation for strip 1 and 2 could be explained by the fact that the recirculation zone is further upstream than observed in the experiments. The simulated streamlines at different Re_L are shown in Figure 7

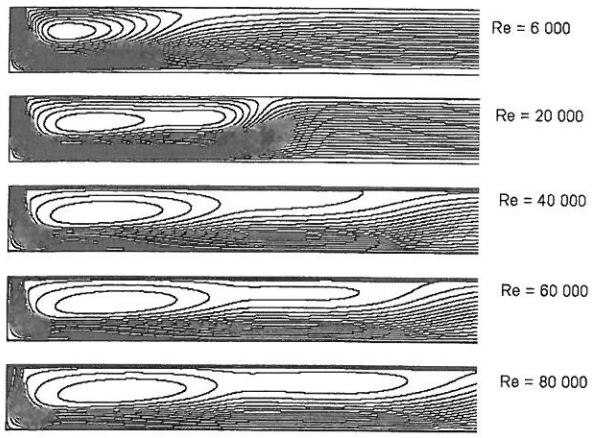

FIGURE 7 Streamlines for different Re_L.

and it is clearly seen that the location and size of the recirculation zone changes with Re_L. Further, the recirculation zone moves downstream as Re_L increases, however, even at higher Re_L the location of the recirculation centre does not reach $x/B = 5$. Again, both the RSM and k-ε over-predict the slope and exhibit an under-prediction of the Nusselt number at lower Reynolds numbers.

The results for strip 1, $x/B = 10$, are shown in Figure 6. The Reynolds number exponent for Nakayama *et al.* (1996) and the RNG k-ε simulation are 0.74 and 0.80, respectively implying that the flow at this strip is close to a turbulent channel flow behaviour. At this location, there is a noted difference between the behaviour of the two experimental data sets, i.e. in the Schafer *et al.* (1991) experiments the Reynolds number exponent is 0.58, which is closer to a laminar boundary layer behaviour. They explain that this is due to the heater downstream being less affected by the recirculation zone. It is possible that in the experiments of Nakayama *et al.* (1996) the recirculation zone was somewhat longer than that of Schafer *et al.* (1991), yielding a higher Nusselt number. It is interesting to note that the k-ε simulation again over-predicts the slope, where as in this region the RSM results yield and exponent similar to the RNG k-ε value.

The predictions indicate that the results downstream of the impingement zone are not in good agreement with the experiments. This could be, at least partially attributed to the jet inlet condition, e.g. that the level of turbulence and the velocity profile. Further, the inaccuracy of the turbulence model downstream of the impingement region could also have a serious impact on the velocity profile (Behnia *et al.*, 1998) and hence the heat transfer coefficient. Shaded contours for the turbulent kinetic energy for $Re_L = 6000$ and 60,000 can be seen in Figure 8. It is noted that for the low Re_L case the maximum is in the impingement region, whereas for the higher Re_L this maximum shifts to the right. This may partially explain the change of the Re_L exponent in the Nusselt correlation. In fact, the results from Nakayama *et al.* (1996) for strip 2 and 1 (Figures 5 and 6) suggest that the flow approaches that of a turbulent channel flow and hence the Re_L exponent P becomes 0.68 and 0.74 for strip 2 and 1, respectively. Further, the numerical results show that the turbulent kinetic energy dissipates halfway across strip 2 for $Re_L = 6000$ and halfway across strip 1 for $Re_L = 60,000$.

Figure 9 shows a comparison of the computed Nusselt number for the impingement strip with correlations obtained by others. The Reynolds number and the Nusselt number are based on the hydraulic diameter of the nozzle ($1.94B$). The present work, Schafer *et al.* (1991) and Nakayama *et al.* (1996) are all confined jet results while Ma and Bergles (1983), Sun *et al.* (1993) and Wolf *et al.* (1990) show free jet results. The present data correlates well with Nakayama *et al.* (1996) and Schafer *et al.* (1991), i.e. there is a reasonable agreement in all confined jet results, whereas unconfined jets exhibit a higher heat transfer rate. It is noted that none of the confined results are for a fully developed jet velocity profile. Behnia *et al.* (1998) have shown that the inlet velocity profile can have a significant effect on the heat transfer coefficient in the impingement region. As noted previously, in the present study the inlet velocity profile is assumed to be uniform.

As the experiments were not truly two-dimensional, numerical simulations with a three-dimensional geometry were also performed for comparison with the two-dimensional results. The intention was

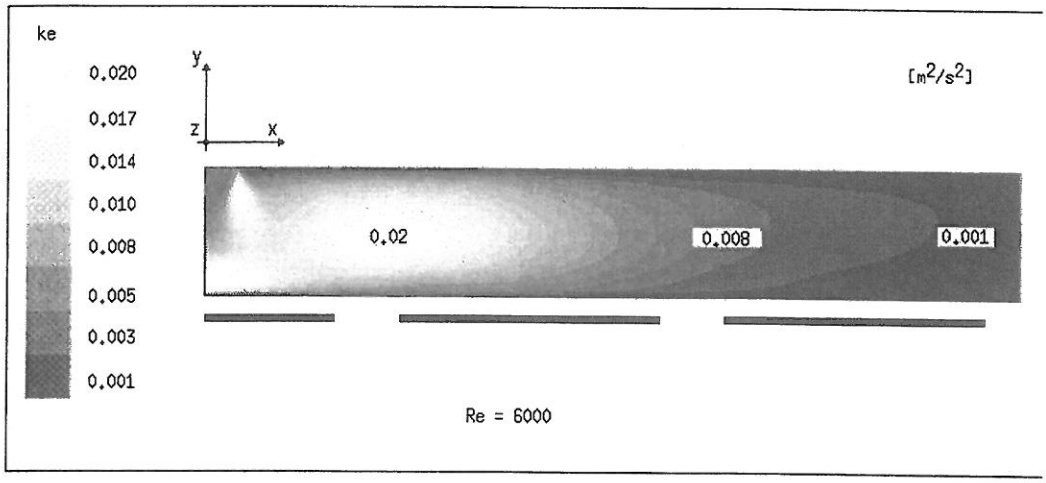

(a)

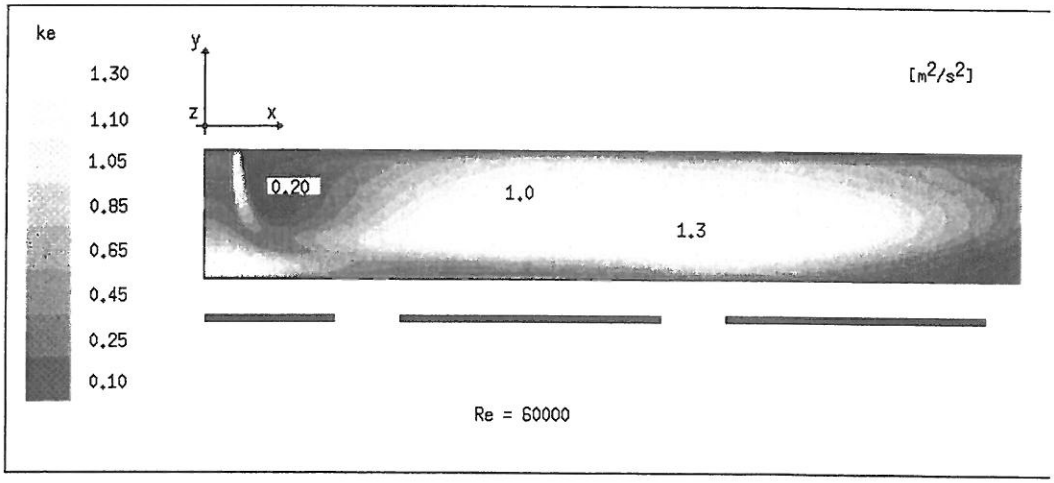

(b)

FIGURE 8 Turbulent kinetic energy, k, for a) $\mathrm{Re}_L = 6000$, b) $\mathrm{Re}_L = 60,000$ (the dark lines represent the strips).

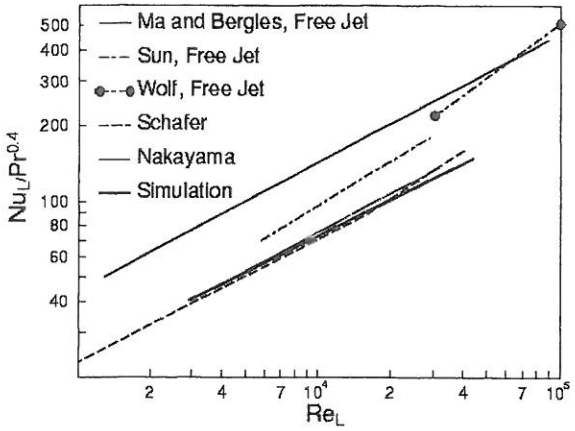

FIGURE 9 Comparison of the average heat transfer coefficient for free and confined jets.

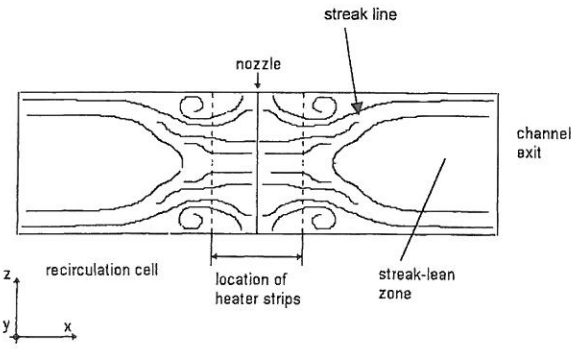

FIGURE 10 Sketch of flow streaks: from Nakayama *et al.* (1996) visualisation experiments using water, $Re_B \approx 10,000$.

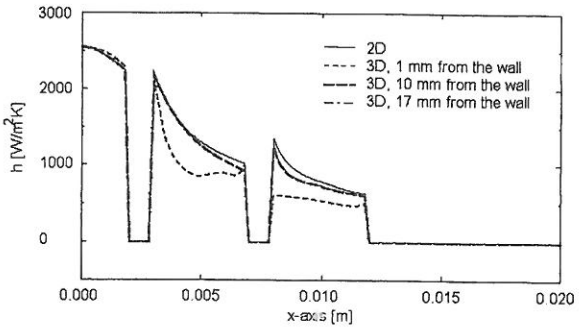

FIGURE 11 Comparison of the 2D and 3D predicted heat transfer coefficient along the x-axis.

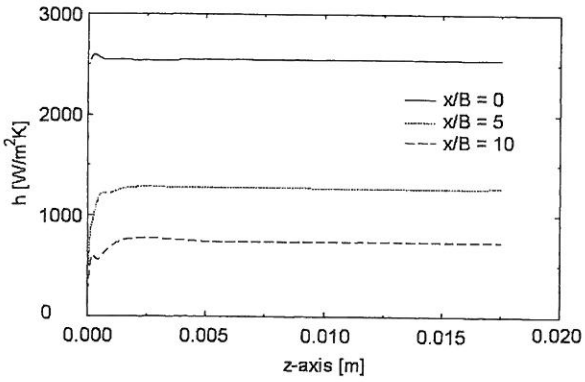

FIGURE 12 The heat transfer coefficient in the z-direction for strips number 1, 2 and 3 (only half of the width is shown, $z = 0.0175$ m is the centre of the flow domain).

to see what additional effects the depth of channel would have on the heat transfer coefficient. Nakayama *et al.* (1996) conducted a separate flow visualisation experiment using a transparent channel with water (instead of FX3250) as the working fluid. Their observations indicated some three-dimensional effects. Most obvious were the recirculation cells near the top and the bottom of the channel, and a "streak-lean" zone that starts about midway between the nozzle and the channel outlet (Figure 10). We used the experimental geometry with around 500,000 cells for the three-dimensional numerical simulation. In Figure 11, the heat transfer coefficient at three different z-planes is compared with the two-dimensional calculation. The grid distribution on these planes is the same as that of the two-dimensional computation. The variation of the heat transfer coefficient across the width of the channel, x-plane, is compared in Figure 12 for the three strips. The effect of the third dimension is not significant. The difference between the 3D and the 2D computation is almost negligible for the centre strip in both the x and z-direction whereas the effect is more pronounced for the strips further downstream. The difference between the 2D and 3D average Nusselt number for the centre strip is negligible, whereas the difference for strips 2 and 1 is 6 and 10%, respectively. This difference can be attributed to the wall effects and the change in the recirculation region downstream of the impingement zone.

TABLE 3 $Nu_L/Pr^{0.4}$ as a function of Re_L

Data set	Strip 3, $x/B = 0$	Strip 2, $x/B = 2$	Strip 1, $x/B = 1$	Re_L $\times 10^{-3}$
Nakayama *et al.* (1996)	$1.1\ Re_L^{0.50}$	$0.16\ Re_L^{0.68}$	$0.078\ Re_L^{0.74}$	8–60
Schafer *et al.* (1991)	$1.5\ Re_L^{0.47}$	$0.32\ Re_L^{0.62}$	$0.250\ Re_L^{0.58}$	6–120
RNG k-ε, 2D Simulations	$1.3\ Re_L^{0.48}$	$0.10\ Re_L^{0.69}$	$0.020\ Re_L^{0.80}$	6–90

CONCLUSIONS

CFD simulations, in a jet impingement/channel flow configuration similar to the experimental geometry of Nakayama *et al.* (1996) for cooling of a series of heated strips, have been performed. Various turbulence models and near-wall treatments were examined. Comparison with experimental data indicated that the RNG k-ε turbulence model and the near-wall treatment using a one-equation model yield the best results. The predicted heat transfer coefficient in the impingement region agreed well with the experimental data, whereas downstream of this region the agreement was not as good. The heat transfer coefficient has been correlated in the form of $Nu_L/Pr^{0.4} = A Re_L^P$ and a summary of the results are presented in Table 3.

For comparison purposes, a 3D simulation was also performed and it was noted that the third dimension did not significantly affect the average heat transfer coefficient. The effect of various parameters of importance (e.g. geometry, turbulence level, flow condition) needs to be further investigated in the future.

In summary, the present study reveals the fact that the current generation CFD code is capable of rendering highly accurate predictions for impinging jet heat transfer even in spatially constrained situations. However, where the flow is supposed to have a complex organization such as in the zone of transition from jet to channel flow, we need to be aware of uncertainties exhibited by Figures 5 and 6.

NOMENCLATURE

$A =$ correlation constant in Eq. 2
$B =$ nozzle width
$H =$ channel spacing
$k_e =$ turbulence kinetic energy
$L =$ strip width
$Nu_L =$ Nusselt number based on the strip width
$P =$ correlation exponent in Eq. 2
$Pr =$ Prandtl number
$Re_L =$ Reynolds number based on the strip width
$Re_y =$ turbulent Reynolds number
$T_j =$ inlet jet temperature
$V_j =$ inlet jet velocity
$h =$ heat transfer coefficient
$k =$ turbulent kinetic energy
$q'' =$ heat flux
$x =$ distance from the centre of the channel to the centre of the heater strip
$y =$ normal distance from the wall to the cell centres
$y^+ =$ dimensionless distance to the wall in Eq. 3
$\rho =$ coolant density
$\lambda =$ thermal conductivity
$\mu =$ dynamic viscosity
$\nu =$ kinematic viscosity
$\tau_w =$ wall shear stress

References

Baughn, J., Mesbah, M. and Yan, X. (1991) An Experimental Study of Entrainment Effects on the Heat Transfer from a Flat Surface to a Heated Circular Impinging Jet, *ASME Journal of Heat Transfer*, **113**, 1023–1025.

Behnia, M., Parneix, S. and Durbin, P. A. (1998) Prediction of Heat Transfer in an Axisymmetric Turbulent Jet Impinging on a Flat Plate, *International Journal of Heat Mass Transfer*, **41**, 1845–1855.

Behnia, M., Parneix, S., Shabany, Y. and Durbin, P. A. (1998) Numerical Simulation of Turbulent Heat Transfer in Confined and Unconfined Impinging Jets, *International Journal of Heat and Fluid Flow*, **20**, 1–9, 1999.

Craft, T., Graham, L. and Launder, B. E. (1993) Impinging Jet Studies for Turbulence Model Assessment-II. An Examination of the Performance of Four Turbulence Models, *International Journal of Heat Mass Transfer*, **36**, 2685–2697.

Ma, C. F. and Bergles, A. E. (1983) Jet Impingement Nucleate Boiling, *International Journal of Heat Mass Transfer*, **29**(8), 1095–1101.

Morris, G. K., Garimella, S. V. and Amano, R. S. (1996) Prediction of Jet Impingement Heat Transfer Using a Hybrid Wall Treatment with Different Turbulent Prandtl Number Functions, *ASME Journal of Heat Transfer*, **118**, 562–569.

Morris, G. K. and Garimella, S. V. (1998) Orifice and Impingement Flow Fields in Confined Jet Impingement, *ASME Journal of Electronic Packaging*, **120**, 68–72.

Mudawar, I. and Wadsworth, D. C. (1991) Critical Heat Flux from a Simulated Chip to a Confined Rectangular Impinging Jet of Dielectric Liquid, *International Journal of Heat Mass Transfer*, **34**(6), 1465–1479.

Nakayama, W., Behnia, M., Mishima, H. and Sun, H. (1996) Heat Transfer from an Array of Strips to Fluorinert Coolant in a Mixed Impinging-Jet/Channel-Flow Configuration, *ASME Journal of Electronic Packaging*, **118**, 31–36.

Nakayama, W. (1997) Liquid-Cooling of Electronic Equipment: Where Does It Offer Viable Solutions?, in *Advances In Electronic Packaging*, Ed. E. Suhir, Y. C. Lee, M. Shiratori and G. Subbarayan, ASME, Vol. 2, pp. 2045–2054.

Schafer, D., Incropera, F. P. and Ramadhyani, S. (1991) Planar Liquid Jet Impingement Cooling of Multiple Discrete Heat Sources, *ASME Journal of Electronic Packaging*, **113**(4), 359–366.

Sun, H., Ma, C. F. and Nakayama, W. (1993) Local Characteristics of Convective Heat Transfer from Simulated Microelectronic Chips to Impinging Submerged Round Water Jets, *ASME Journal of Electronic Packaging*, **115**(1), 71–77.

Willingham, T. C. and Mudawar, I. (1992) Channel Height Effects on Forced-Convection Boiling and Critical Heat Flux from a Linear Array of Discrete Heat Sources, *International Journal of Heat Mass Transfer*, **35**(8), 1865–1880.

Wolf, D. H., Viskanta, R. and Incropera, F. P. (1990) Local Convective Heat Transfer from a Heated Surface to a Planar Jet of Water with a Non Uniform Velocity Profile, *ASME Journal of Heat Transfer*, **112**, 899–905.